Homo-FRET Microscopy in Living Cells to Measure Monomer-Dimer Transition of GFP-Tagged Proteins

I. Gautier,* M. Tramier,* C. Durieux,* J. Coppey,* R. B. Pansu,† J-C. Nicolas,‡ K. Kemnitz,§ and M. Coppey-Moisan*

*Institut Jacques Monod, Centre National de la Recherche Scientifique, Université P6/P7, 75251 Paris, France; †Laboratoire de Photophysique et Photochimie Macromoléculaires et Supramoléculaires, 94235 Cachan, France; ‡Service de Microbiologie, Hôpital Rothschild, 75571 Paris, France; and §EuroPhoton GmbH, D-12247, Berlin, Germany

ABSTRACT Fluorescence anisotropy decay microscopy was used to determine, in individual living cells, the spatial monomer-dimer distribution of proteins, as exemplified by herpes simplex virus thymidine kinase (TK) fused to green fluorescent protein (GFP). Accordingly, the fluorescence anisotropy dynamics of two fusion proteins (TK_{27}GFP and TK_{366}GFP) was recorded in the confocal mode by ultra-sensitive time-correlated single-photon counting. This provided a measurement of the rotational time of these proteins, which, by comparing with GFP, allowed the determination of their oligomeric state in both the cytoplasm and the nucleus. It also revealed energy homo-transfer within aggregates that TK_{366}GFP progressively formed. Using a symmetric dimer model, structural parameters were estimated; the mutual orientation of the transition dipoles of the two GFP chromophores, calculated from the residual anisotropy, was 44.6 $\pm$ 1.6°, and the upper intermolecular limit between the two fluorescent tags, calculated from the energy transfer rate, was 70 Å. Acquisition of the fluorescence steady-state intensity, lifetime, and anisotropy decay in the same cells, at different times after transfection, indicated that TK_{366}GFP was initially in a monomeric state and then formed dimers that grew into aggregates. Picosecond time-resolved fluorescence anisotropy microscopy opens a promising avenue for obtaining structural information on proteins in individual living cells, even when expression levels are very low.

INTRODUCTION

Quantitative information on protein structure in living cells is a prerequisite for a full understanding of cellular processes. X-ray crystallography and multidimensional NMR spectroscopy are powerful methods for determining the three-dimensional structure of proteins, but not yet for studying proteins directly in living cells. Fluorescence microscopy, especially the time-correlated variant, is currently the most sensitive and versatile method for live cell studies. Fluorescence resonance energy transfer (FRET) between a fluorescent donor and an acceptor molecule has been widely used to determine distances in macromolecules and thus to obtain structural information (Stryer, 1978; Van der Meer et al., 1994). FRET between spectrally different chromophores (hetero-FRET) has opened the way to studying protein interactions (Llopis et al., 2000; Mahajan et al., 1998) and biochemical reactions (Ng et al., 1999; Nagai et al., 2000; Emmanouilidou et al., 1999; Vanderklish et al., 2000; Bastiaens and Squire, 1999) in living cells by taking advantage of the various spectrally shifted fluorescent proteins.

FRET can also occur between like chromophores (homo-FRET). This process, which can only be monitored by fluorescence anisotropy (Weber, 1954), was used recently to study protein structure (Bastiaens et al., 1992) and oligomerization (Runnels and Scarlata, 1995; Blackman et al., 1998) and the organization of membrane proteins in submicrodomains at the cell surface (Varma and Mayor, 1998). Moreover, time-resolved fluorescence anisotropy measurements allowed the determination of the rate of intramolecular (or intermolecular) energy migration and therefore the calculation, under certain circumstances, of the average distance between the chromophores (Bergström et al., 1999; Bastiaens et al., 1992) and the determination of structural data on protein-ligand complexes in solution (Wilczynska et al., 1997).

We show here that picosecond time-resolved fluorescence anisotropy microscopy can be an excellent method for determining subcellular monomer-dimer transitions and the oligomerization of proteins within living cells. Homo-FRET between identical green fluorescent protein (GFP) chromophores fused to monomers of herpes simplex virus (HSV-1) thymidine kinase (TK) was unveiled and followed directly in living cells. The TK of HSV-1 phosphorylates a wide range of nucleoside analogs, forming the basis of selective anti-herpes and viral vector-based gene therapies. Crystallized in the presence of substrate, TK of HSV-1 forms homo-dimers (Wild et al., 1997), which are thought to be the active form (Fetzer et al., 1994; Waldman et al., 1983). The ultra-sensitive time-correlated single-photon counting (TCSPC) (O'Connor and Phillips, 1984) microscopy was applied to measure fluorescence anisotropy decays (Tramier et al., 2000) of GFP-tagged TK derivatives in living cells and to determine their oligomeric state.

Time-resolved fluorescence anisotropy monitors any process that changes the polarization of the emitted fluores-

Received for publication 29 September 2000 and in final form 15 March 2001.

Address reprint requests to Dr. Maïté Coppey-Moisan, Institut Jacques Monod, UMR 7592, 2 Place Jussieu-Tour 43, 75251 Paris Cedex 05, France. Tel.: 33-1-44-27-79-51; Fax: 33-1-44-27-79-51; E-mail: maite.coppey@ijm.jussieu.fr.

0006-3495/01/06/3000/09 $2.00

cence during the excited state. Consequently, the fluorescence anisotropy decay is influenced 1) by rotational movements of the fluorescent molecules and 2) by energy transfer taking place within the fluorescence time scale (if it occurs). Both aspects of anisotropy dynamics were used in the present work to determine 1) the rotational diffusion of the GFP-tagged TK derivatives in subcellular compartments and 2) the occurrence of homo-transfer between GFP moieties, which allowed us to show a transition from monomeric to dimeric forms directly in living cells.

MATERIALS AND METHODS

Construction of fusion proteins

The pTK14 expression vector for HSV-1 TK was kindly provided by I. Pelletier and F. Colbere-Garapin (Institut Pasteur, Paris, France). Two plasmids encoding various lengths of the N-terminal part of TK fused to GFP, under the control of the TK promoter, were constructed. GFP (pEGFP-C1, Clontech, Montigny le Bretonneux, France) was amplified by polymerase chain reaction (PCR) with two different upstream primers (5′-AAAAAACGTACGGTGAGCAAGGGCGAGG-3′, 5′-AAAAAAGCGCGCGTGAGCAAGGGCGAGG-3′) and one downstream primer (5′-AAAAAAGCGCGCCTTGTACAGCTCGTCC-3′). The two different PCR products were subcloned between the *Spl*I and *BssH*II sites, and in the *BssH*II site of pTK14, respectively. The resulting plasmids coded for GFP fused to the 27 N-terminal residues ($pTK_{27}GFP$) and the 366 N-terminal residues ($pTK_{366}GFP$) of TK, respectively. Using PCR, a 6xHis tag was added to the C-terminal extremity of each fusion protein; the upstream (6xHis tag-encoding) primer was 5′-AACCCGGGAGCATCATCATCATCATCATTGAAACACGGAAGGAG-3′ and the downstream primer, hybridizing downstream of the TK polyA, was 5′-GTACATGCGGTCCATGCCCA-3′. The fragment was inserted between the *Sma*I and *Tth111*I sites. These plasmids were digested with *Pvu*II and *EcoR*I, and the fragments corresponding to the *tk* and *gfp* genes were subcloned between the *EcoR*I and *EcoR*V sites of pcDNA3.1 (Invitrogen, Groningen, The Netherlands), to express the fusion proteins under control of the cytomegalovirus promoter. All clones were confirmed by sequencing.

Expression of fusion proteins

Vero and COS-7 cells were cultured on glass coverslips in Dulbecco's modified Eagle's medium (Life Technologies, Cergy Pontoise, France), supplemented with fetal calf serum (10%), at 37°C in 5% CO_2 atmosphere. The cells were transfected with pEGFP-C1 or the TK plasmids, using FuGENE 6 Transfection Reagent (Roche Molecular Biochemicals, Meylan, France), according to the manufacturer's instructions. The cells expressing the fusion proteins were detected by fluorescence techniques described below.

Steady-state fluorescence microscopy at low light level

Fluorescence imaging was carried out in epi-fluorescence using an inverted microscope (Leica DMIRBE, Rueil Malmaison, France) at room temperature. The coverslips mounted in an open observation chamber were imaged through a 100× (NA = 1.3) ultra-fluor objective. The detector was a cooled slow-scan CCD camera with 1160 × 1040 pixels, digitized on a 4096 level gray scale (SILAR, St. Petersburg, Russia). Low excitation light levels were used to prevent photodynamic perturbations in the cells. For GFP fluorescence, $\lambda_{exc} = 480$ nm, OD = 2, and 515 nm $< \lambda_{em} <$ 560 nm. Background subtraction and shading correction were carried out as described elsewhere (Coppey-Moisan et al., 1994) using Khoros software (Khoral Research, Albuquerque, NM).

Fluorescence lifetime, anisotropy decay microscopy, and data analysis

The confocal microscope used for measuring of fluorescence dynamics has been described in detail elsewhere (Tramier et al., 2000). Briefly, a titanium-sapphire picosecond laser beam (Tsunami, Spectra Physics France, les Ulis, France), $\lambda_{exc} = 493$ nm and 4 MHz, after passing through a frequency doubler and a pulse picker, was directed through the light-inlet port of a Nikon epi-fluorescence inverted microscope. The fluorescence photons emitted from the illuminated volume of 1 μm^3 were collected by a 100× objective (NA = 1.3) and conducted through an optic fiber (400 μm diameter) to a TCSPC detector (Hamamatsu Photonics France, R3809U, Massy, France). Different subcellular localizations of the excited volume (cytoplasm and nucleus) were chosen to measure fluorescence decays. A Fresnel rotator was placed in the excitation laser beam and a polarizer sheet before the optical fiber in the emission path. The optical design of the microscope results in four geometric components of the fluorescence polarization, where i_{vh} and i_{hv} pertain to the parallel direction and i_{vv} and i_{hh} to the perpendicular direction, relative to the direction of laser excitation. For anisotropy measurements, parallel ($i_{vh}(t)$) and perpendicular ($i_{hh}(t)$) decays were acquired sequentially from the same sample spot. The two decays were normalized as described previously (Tramier et al., 2000). The normalized experimental decays, $i^N_{vh}(t)$ and $i^N_{hh}(t)$, are distorted by the measurement apparatus and are related to the real-time behavior, $i_{par}(t)$ and $i_{per}(t)$, by the convolution product of the instrument response function IRF(t):

$$i^N_{vh}(t) = \mathrm{IRF}(t) \times i_{par}(t) \tag{1}$$

and

$$i^N_{hh}(t) = \mathrm{IRF}(t) \times i_{per}(t) \tag{2}$$

The anisotropy function $r(t)$ is defined by

$$r(t) = D(t)/S(t), \tag{3}$$

where

$$D(t) = i_{par}(t) - i_{per}(t) \tag{4}$$

is the difference between the parallel and the perpendicular decay, and

$$S(t) = i_{par}(t) + 2i_{per}(t) \tag{5}$$

is the decay of total intensity.

By combining Eq. 3, 4, and 5:

$$3i_{par}(t) = S(t)[1 + 2r(t)] \tag{6}$$

and

$$3i_{per}(t) = S(t)[1 - r(t)]. \tag{7}$$

For GFP (S65T mutant), the total intensity decay is monoexponential in solution (Volkmer et al., 2000) and in living cells (our data). $S(t)$ can be fitted with the model function:

$$S(t) = 3ae^{-t/\tau}, \tag{8}$$

where τ is the fluorescence lifetime and a is a constant.

To fit the experimental data, two phenomenological functions were used:

$$r(t) = r_0 e^{-t/\Phi} \tag{9}$$

or

$$r(t) = r_0[(1 - b)e^{-t/\Phi 1} + be^{-t/\Phi 2}], \quad (10)$$

where r_0 is the initial anisotropy, Φ_i are correlation times, and b is a constant.

The two normalized experimental decays were fitted by a Marquardt nonlinear least-square algorithm, using the expressions

$$i_{vh}^N(t) = \mathrm{IRF}(t) \times [ae^{-t/\tau}(1 + 2r_0e^{-t/\Phi})] \quad (11)$$

and

$$i_{hh}^N(t) = \mathrm{IRF}(t) \times [ae^{-t/\tau}(1 - r_0e^{-t/\Phi})] \quad (12)$$

or, if the experimental data are better fitted with a two-exponential anisotropy decay,

$$i_{vh}^N(t) = \mathrm{IRF}(t) \times [ae^{-t/\tau}(1 + 2r_0((1 - b)e^{-t/\Phi 1} + be^{-t/\Phi 2}))] \quad (13)$$

and

$$i_{hh}^N(t) = \mathrm{IRF}(t) \times [ae^{-t/\tau}(1 - r_0((1 - b)e^{-t/\Phi 1} + be^{-t/\Phi 2}))]. \quad (14)$$

Analysis was performed with Global analysis software (Globals Unlimited, Urbana, IL). Static background, as measured by the mean number of counts before the rise of fluorescence, was treated as a fit-parameter by the kinetic analysis software. The dynamic background was measured from a background sample (e.g., a nontransfected cell) under identical conditions and incorporated in the analysis.

THEORETICAL BACKGROUND

The Förster mechanism of electronic energy transfer (Förster, 1948) can occur between like chromophores if these molecules are close enough ($R < \sim 1.6R_0$, the Förster radius), for example, in the case of a dimer of fluorescent-tagged proteins. Because the photophysical properties of the two donor molecules are the same, the excitation energy is reversibly transferred between the fluorescent tags. This transfer does not change fluorescence lifetime properties and can be monitored only by fluorescence anisotropy.

The energy transfer between like chromophores in the case of dimers composed of identical monomers is assumed to take place in the fluorescent states, from initially excited state i to state j and reversibly from j to i with the same rate constant, ω. Assuming that 1) the dimers are equivalent to each other (a symmetrical configuration) and their orientation is distributed randomly in the observation volume ($\sim 1\ \mu m^3$); 2) the rotation of the protein dimer during the fluorescence lifetime is negligible; and 3) there is no reorientation of the absorption transition moment relative to the initially excited state i or to the secondary excited state j, and no reorientation of the emission transition moment of state i and state j during the lifetime of the fluorophore (static model); i.e., angular variables in the transition moments are independent of time, then the excitation energy migration from electronic state i to j (and j to i) contributes to the time-dependent fluorescence anisotropy, $r(t)$, and

$$r(t) = 3/20(2\cos^2\delta - \cos^2\theta_{ij} - \cos^2\theta_{ji})e^{-2\omega t} + 1/20(6\cos^2\delta + 3\cos^2\theta_{ij} + 3\cos^2\theta_{ji} - 4), \quad (15)$$

where δ is the intramolecular angle between the absorption and emission transition moments, and θ_{ij} and θ_{ji} are the static mutual orientations of the transition moments of absorption to state i and of emission from state j, and between those of absorption to j and emission from i, respectively, as described by Tanaka and Mataga (1979).

In the case of the GFP chromophore, the absorption and emission transition moments are parallel (Volkmer et al., 2000). Thus, $\delta = 0$, and $\theta_{ij} = \theta_{ji} = \theta$.

The time-dependent anisotropy thus becomes

$$r(t) = 1/10[(3 - 3\cos^2\theta)e^{-2\omega t} + 3\cos^2\theta + 1]. \quad (16)$$

In the static limits (no reorientation of the transition moments during the fluorescence lifetime), the transfer rate is linked to the distance R between the two interacting chromophores by

$$\omega = 3/2\langle\kappa^2\rangle(R_0/R)^6\tau^{-1}, \quad (17)$$

where the average angular dependence of dipole-dipole coupling $\langle\kappa^2\rangle$ (with the assumptions made in the model) is equal to

$$\langle\kappa^2\rangle = (\cos\theta - 3\cos^2\beta)^2, \quad (18)$$

where θ is the mutual orientation between the two chromophores and β is the angle between the separation vector R and the transition moment of the chromophore.

R_0, the dynamical averaged Förster radius, is a function of the spectral properties of the chromophore as given by

$$R_0 = (8.79 \times 10^{-5}J \times 2/3 \times Q_D n^{-4})^{1/6}\ \text{Å}, \quad (19)$$

where Q_D is the donor quantum yield, n the refractive index, and J the spectral overlap integral, calculated from the donor fluorescence (f_D) and acceptor absorption (ε_A) spectra:

$$J = \int f_D(\lambda)\ \varepsilon_A(\lambda)\ \lambda^4\ d\lambda \Big/ \int f_D(\lambda)\ d\lambda. \quad (20)$$

In the absence of energy transfer, for a fluorescent molecule covalently linked to a globular protein molecule under conditions in which the fluorophore does not undergo rotational motion during the excited state lifetime, the orientational correlation function can be written as

$$r_i(t) = r_0e^{-t/\Phi}, \quad (21)$$

where Φ denotes the rotational correlation time of the protein molecule and r_0 the anisotropy at time 0. Φ is

correlated to the hydrodynamic volume of the protein V by the Stokes-Einstein equation:

$$\Phi = \eta V/kT,$$

where η is the viscosity of the medium, k the Boltzmann's constant, and T the temperature.

RESULTS AND DISCUSSION

Subcellular steady-state and time-resolved fluorescence distribution of GFP-tagged TK derivatives: patterns of protein expression at the single-cell level

GFP (S65T) was fused to the carboxyl terminus of the TK of HSV-1, shortened by 10 ($TK_{366}GFP$) or by 349 ($TK_{27}GFP$) amino acids. The transient expression of the two fusion proteins, governed either by the TK promoter in Vero cells or by the cytomegalovirus promoter and amplified by means of the SV40 *ori* in COS-7 cells, was monitored by fluorescence microscopy. Diffuse fluorescence was detected in the cytoplasm (weak fluorescence for $TK_{366}GFP$) and in the nucleus (Fig. 1, *a* and *c*) for the two fusion proteins as was for GFP (not shown). For $TK_{366}GFP$, an additional punctate green fluorescence appeared in a proportion of cells, which increased with time after transfection (Fig. 1 *b*). This punctate fluorescence is assumed to result from aggregated proteins, because the size and number of these structures increased with time. These distinct fluorescence patterns clearly localized differently from lysosomes or endosomes labeled by LysoTracker Red DND-99 (Molecular Probes Europe, Leiden, The Netherlands) (not shown), demonstrating that the aggregates were not targeted to the lysosomal degradation pathway. The subcellular fluorescence pattern for both proteins was independent of the cell type and the expression vector.

Fluorescence decays were collected from diffuse and punctate areas of the cytoplasm and nucleus by the TCSPC method (O'Connor and Phillips, 1984) under the microscope (Tramier et al., 2000). The fluorescence decays were monoexponential, with a lifetime of 2.6 ± 0.1 ns (Table 1), in good agreement with previous values obtained in cells with a different technique (Swaminathan et al., 1997; Pepperkok et al., 1999). However, recent experiments carried out with the S65TGFP mutant in solution and using TCSPC gave either a different lifetime value (Volkmer et al., 2000) or even three lifetimes (Hink et al., 2000). These discrepancies could arise from different protein folding due to extraction and purification procedures. The existence of several lifetimes (Hink et al., 2000) could be explained by photo-conversion processes, as previously evidenced for GFPs (Creemers et al., 2000; Volkmer et al., 2000). At

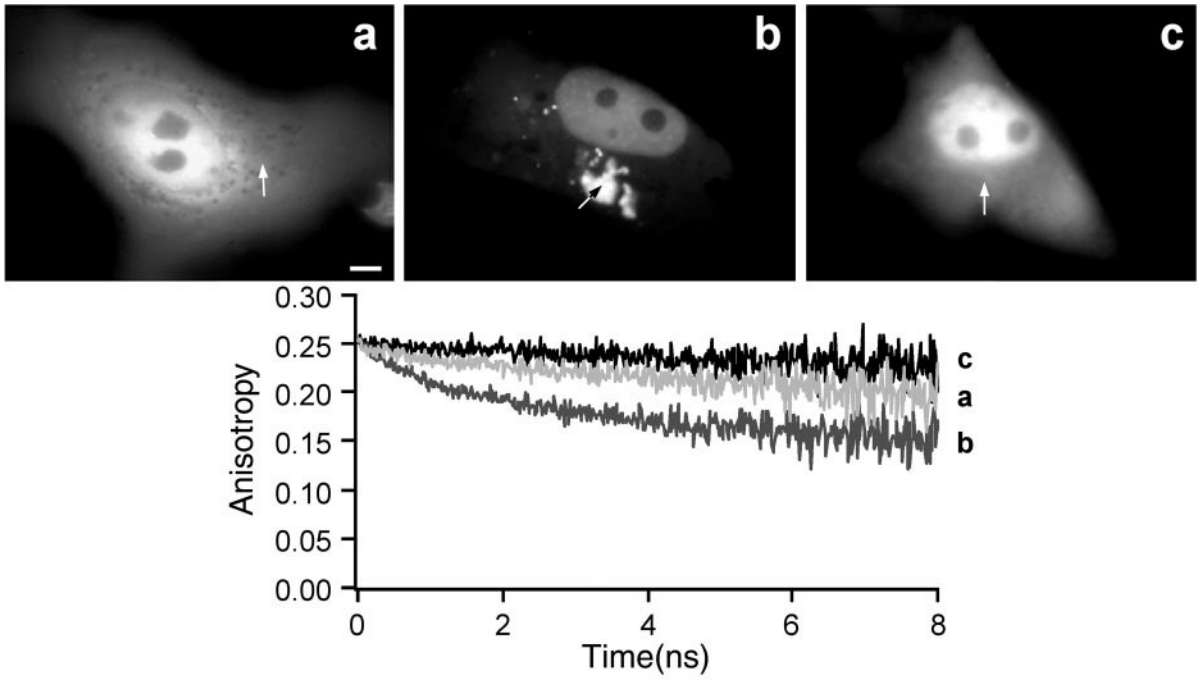

FIGURE 1 Subcellular fluorescence anisotropy decays of $TK_{27}GFP$ and $TK_{366}GFP$ proteins. (*Top*) Steady-state fluorescence images of Vero cells expressing $TK_{27}GFP$ (*a*) and $TK_{366}GFP$ (*b* and *c*). (*a* and *c*) Cells presenting only a diffuse cytoplasmic and nuclear fluorescence pattern; (*b*) Cells containing fluorescent aggregates. (*Bottom*) Time-resolved fluorescence depolarization from a cytoplasmic area of diffuse fluorescence (*a* and *c*) and from an area inside an aggregate (*b*). The subcellular location of the illuminated volume (~1 μm^3) from which the anisotropy decay was performed is indicated by an arrow. For cells containing aggregates, anisotropy decays from nuclear or cytoplasmic area of diffuse fluorescence were similar to that obtained from aggregates (*b*). Bar in *a*, 5 μm.

TABLE 1 Fluorescence dynamics parameters of GFP and GFP-tagged TK derivatives expressed in living cells

Protein	Lifetime (ns)	Initial anisotropy r_0	Relaxation time Φ_1 (ns)	Relaxation time Φ_2 (ns)	Anisotropy contribution of Φ_2	Number of experiments
GFP	2.58 ± 0.02	0.26 ± 0.01	23.4 ± 2.3			6
$TK_{27}GFP$	2.62 ± 0.09	0.26 ± 0.02	34.6 ± 9.0			6
$TK_{366}GFP$	2.47 ± 0.20	0.26 ± 0.01	81.0 ± 15.3			3(a)
		0.23 ± 0.01	2.4 ± 0.3	≥200	0.63 ± 0.02	3(b)

$TK_{27}GFP$ and $TK_{366}GFP$ represent the 27 and 366 N-terminal amino acids of the herpes simplex virus type 1 thymidine kinase fused to GFP, respectively. Errors are standard deviations. a and b represent anisotropy decay parameters of cells without and with aggregates, respectively. The anisotropy contribution of Φ_2 corresponds to the parameter b in Eq. 10. The r_0 values are similar to the value previously determined by microscopy with 1.3 numerical aperture of the objective for a chromophore where the orientations of the excitation and emission dipole are identical (Tramier et al., 2000).

present, we cannot completely exclude the occurrence of small contributions (<25%) of shorter lifetime components in our experiments.

Fluorescence anisotropy decay from subcellular areas: rotational time and homo-FRET measurements

Quantitative steady-state and fluorescence lifetime measurements cannot discriminate between free GFP and GFP-tagged TK proteins, nor reveal the oligomeric state of proteins. Therefore, the dynamics of fluorescence anisotropy was followed 1) to monitor the rotational behavior of the proteins and 2) to study macromolecular interactions by measurement of potential homo-FRET. Fluorescence anisotropy decays were measured as described in Materials and Methods and as previously described (Tramier et al., 2000). Typical fluorescence anisotropy decays are displayed in Fig. 1. For $TK_{27}GFP$, a single decay curve was observed (Fig. 1 *a*), whatever the subcellular localization, the time elapsed after transfection, and the steady-state fluorescence level. For $TK_{366}GFP$, two different fluorescence anisotropy decays were observed according to the presence (Fig. 1 *b*) or absence (Fig. 1 *c*) of subcellular aggregates.

As a control, the fluorescence anisotropy decay of free GFP was measured in the same type of living cells and under the same experimental conditions as for the GFP-tagged TK derivatives. The fluorescence anisotropy decay curves for both the GFP-tagged TK derivatives shown in Fig. 1, *a* and *c*, and GFP could be fitted as monoexponential decays. Such dynamics of anisotropy are relevant to rotational diffusion of the fluorescent proteins (see Eq. 21). The rotational parameters obtained from the fit with Eqs. 11 and 12 are displayed in Table 1.

The fluorescence anisotropy decay measurements were carried out under the microscope using a high-numerical-aperture (NA = 1.3) objective. As predicted by Axelrod (1979, 1989) and experimentally verified by Tramier et al. (2000), the decrease of r_0 from 0.4 to 0.23 (Table 1) corresponded to the depolarization by the optical set-up of the microscope. However, this depolarization did not change the kinetic parameters obtained from fluorescence decays and fluorescence anisotropy decays (Tramier et al., 2000). The rotational time calculated for GFP (23 ns) gives an apparent volume corresponding to a sphere of 50 Å in diameter when assuming a subcellular viscosity of 1.5 cp, as measured elsewhere (Swaminathan et al., 1997) (from Eq. 22, Theoretical Background). The theoretical value for the apparent diameter of GFP assimilated to a sphere, based on a 27-kDa molecular mass and a hydrated volume of a protein of $\sim 1\ cm^3\ g^{-1}$ (Cantor and Schimmel, 1980), would be 44 Å. Thus, it is likely that GFP was monomeric in the living cells studied here. Rotational times of 34 ns and 81 ns were obtained, respectively, for $TK_{27}GFP$ and $TK_{366}GFP$ (in cells without aggregates) (Table 1), which are in fair agreement with 1) the apparent volume corresponding to the theoretical size of each chimeric protein and 2) GFP-tagged TK derivatives being monomeric (assuming the same subcellular viscosity). The increasing rotational time with the size of the protein showed that the cytoplasmic and nuclear fluorescence arose from the fusion protein and not from potentially cleaved GFP. These different Φ values are particularly critical to discriminate GFP and GFP-tagged proteins. The fluorescence anisotropy decays (Fig. 1, *curves a* and *c*) do not completely relax during the time window of the measurements, because the rotational time of GFP-tagged proteins is more than 10-fold longer than the fluorescence lifetime. Despite this intrinsic limitation, the individual polarized intensity components were simultaneously fitted so that the information of the whole decay curves was exploited. The fits of these decays lead to an anisotropy that tends toward zero at long times, meaning that no protein would have hindered rotation, which would have been due to interactions with subcellular macromolecular components.

In contrast, in cells transfected with $TK_{366}GFP$ containing punctate green fluorescence, anisotropy decays obtained from the aggregates or from diffuse fluorescence (cytoplasmic and nuclear; Fig. 1 *b*) required a biexponential relaxation model (Eq.10; see Materials and Methods). The fit parameters, obtained from Eqs.13 and 14 and reported in Table 1, indicated a rapid anisotropy relaxation time, Φ_1 = 2.4 ± 0.3 ns, for 37% and a very long relaxation time, Φ_2

$\geq$ 200 ns, for 63%. The rapid anisotropy relaxation, occurring at short times, cannot be ascribed to any rotational motion. For instance, free GFP, if any (which could have been cleaved in aggregates), would give a rotational time of 23 ns, greater than the relaxation time of 2.4 ns (see Table 1). Local motion of the chromophore within its barrel-shaped pocket can be ruled out, too, because it should also result in a reduced fluorescence lifetime. Bending motions of the peptide region linking the two proteins would be expected to give a correlation time longer than 2.4 ns, as was shown recently (Hink et al., 2000), and it should be observed with the anisotropy decay of the monomer, which was not the case (Fig. 1 *c*). This fast depolarization is typical of Förster-type resonance energy transfer (FRET) between like chromophores. Homo-transfer does not change spectral and lifetime properties of the emitted fluorescence, but leads to depolarization (Weber, 1954). It is likely that this homo-transfer between GFP chromophores reflects dimer formation of $TK_{366}GFP$.

Quantification of homo-FRET between the two GFP chromophores within the $TK_{366}GFP$ dimers in living cells

In the presence of energy transfer between two identical chromophores, time-dependent fluorescence anisotropy is correlated with the transfer rate, ω, and with the mutual orientation of the two chromophores, θ, by Eq. 16, as described in Theoretical Background. This equation relies on several assumptions that seem to hold true for $TK_{366}GFP$ in living cells. First, the rotation of the protein dimer during the fluorescence lifetime is negligible. Indeed, the rotational time of the monomer has been estimated to be 81.0 $\pm$ 15.3 ns, which gives a value of $\sim$162 ns for the rotation of the dimer. Because the de-excitation process of GFP is faster (2.6 ns), it was impossible to discriminate between rotation of the dimer and a motionless molecule. Second, there is no reorientation of the transition moments of both initially and secondarily excited states during the fluorescence lifetime (static model). Indeed, the GFP chromophore is rigidly fixed inside the barrel because rapid motion was evidenced neither in vitro (Volkmer et al., 2000) nor here in the living cell. Moreover, the GFP moieties themselves do not move significantly, because no such rotation could be evidenced in the fluorescence anisotropy decay of the $TK_{366}GFP$ monomer. And third, as the GFP tag was added to the TK part by genetic engineering from a single recombinant plasmid, the monomers were identical. It is likely that the orientation of GFP chromophores was symmetrical within the dimer.

Interestingly, with this model, the anisotropy does not fall to zero at long times, but goes to a residual anisotropy, r_∞ (equal to $1/10(3\cos^2\theta + 1)$). The value of $\Phi_2 \geq$ 200 ns could be interpreted as the residual anisotropy in the context of a one-step energy migration between two GFP chromophores within dimers. However, it cannot be excluded that the measured transfer rate corresponded to one average of a distribution of transfer rates, the transfer taking place between ordered protein clusters of higher stoichiometry.

The physical parameters, obtained from Eq. 16 for $TK_{366}GFP$ forming aggregates in living cells, are shown in Table 2. Similar results were obtained in cells containing aggregates over the area of diffuse fluorescence of $TK_{366}GFP$. These results show that homo-FRET was also unveiled in a diffuse fluorescence area, suggesting that $TK_{366}GFP$ dimerization was more likely to occur than protein clusters.

From the experimental value of r_∞, the angle θ, corresponding to the mutual orientation between the two GFP chromophores, was determined and found to be equal to 44.6 $\pm$ 1.6°. From the value of the transfer rate, ω, the distance between the two interacting chromophores, R, can be calculated if the orientational factor, $\langle\kappa^2\rangle$, is known (Eq. 17). $\langle\kappa^2\rangle$ depends on the mutual orientation of the transition dipoles of the two chromophores, θ, and also on their orientation with respect to the axis joining the two chromophores (see Eq. 18). This last orientation is unknown.

A random value of $\langle\kappa^2\rangle$ cannot be taken into account because no random local motion of GFP or its chromophore was detected. The minimal value of R corresponds to the situation in which the two GFP barrels are in contact. In this case, the minimal distance between the two GFP chromophores is 24 Å, the smallest GFP barrel dimension. The upper limit of R was calculated from the maximal value of κ^2, i.e., 4 (Table 2). For the calculation, the dynamically averaged Förster radius (computed with an effective orientational factor of 2/3), R_0 = 47 Å, was obtained from the overlap of the absorption and emission spectra of GFP, using 58,000 M^{-1} cm^{-1} as absorption coefficient at the maximum, 0.66 as GFP quantum yield, and 1.33 as the refractive index of the medium (from Eq. 19). The calculated value of R = 70 Å is compatible with the known dimeric structure of TK obtained by x-ray diffraction from the crystallized form. Indeed, within crystallized TK dimer, the two carboxyl termini of the TK dimer are 47 Å apart (G. E. Schulz, Freiburg im Breisgau, Germany, personal communication).

TABLE 2 Physical parameters of energy transfer between GFP chromophores within $TK_{366}GFP$ dimers in living cells

Independent experiment number	θ	ω (ns^{-1})	R (Å)
1	44.6°	0.208	70.2
2	43.8°	0.185	71.6
3	46.1°	0.238	68.6

θ, the mutual orientation between the two GFP chromophores, and ω, the energy transfer rate, are calculated from Eq. 16, R, the upper limit of the distance between the two GFP chromophores, is calculated from Eq. 17 with $\kappa^2 = 4$.

Dimerization and aggregation of $TK_{366}GFP$ are specific to the TK part and independent of the expression level

Because the fluorescence lifetimes were shown to be similar for GFP and GFP-tagged TK derivatives for all the different subcellular patterns (Table 1), the steady-state fluorescence intensity could be assumed to be proportional to the amount of protein. Thus, quantification of the fusion proteins or GFP expression at the single-cell level could be carried out. Even when GFP was expressed at high levels (this occurred in COS-7 cells), no aggregates were detected, in contrast to what was observed with $TK_{366}GFP$ at much lower expression (Fig. 2). This indicates that the formation of aggregates, observed with $TK_{366}GFP$, is driven by the TK part and not by GFP-GFP interactions. Homo-FRET was observed for aggregated $TK_{366}GFP$ but not for GFP, whatever its expression level in single living cells (not shown). This contrasts with wild-type GFP, which, in solution, self-associates with increasing concentration (Ward et al., 1982).

Twenty-four hours after transfection, the aggregates appeared as small (actual dimension being probably smaller than the optical resolution, i.e., 0.2 μm) bright spots in a few cells. The following days, the number and the size of these aggregates and the proportion of cells with aggregates increased. The aggregates could reach a huge size (3–5 μm in diameter, as shown in Fig. 1 *b*) in the cytoplasm and nucleus. However, the growth of the aggregates did not depend on the level of protein expression (shown in Fig. 3). The total steady-state fluorescence per cell, which was proportional to the amount of expressed $TK_{366}GFP$ (see above), was not correlated with the presence of aggregates. As $TK_{366}GFP$ dimers occurred in cytoplasmic and nuclear diffuse fluorescence areas in cells containing aggregates, it is likely that $TK_{366}GFP$ aggregation proceeds from the soluble dimer.

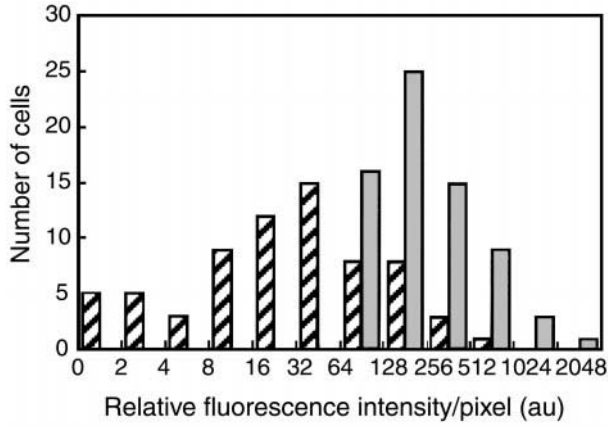

FIGURE 2 Histograms of fluorescence intensity of GFP expressed in COS-7 cells (*shaded bars*) and of $TK_{366}GFP$ expressed in aggregate-containing Vero cells (*hatched bars*). The fluorescence intensity was measured over the whole cell area. Because the fluorescence lifetimes were independent of the protein, alone or fused (see Table 1), and of the cell type, the steady-state fluorescence intensity per cell was proportional to the amount of expressed protein.

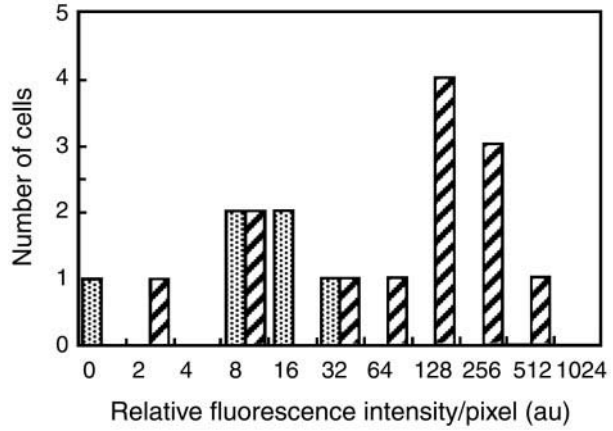

FIGURE 3 Histograms of fluorescence intensity of $TK_{366}GFP$ expressed in Vero cells with aggregates (*hatched bars*) or without aggregates (*spotted bars*).

CONCLUSION

The time-correlated fluorescence experiments, carried out with GFP and GFP-tagged TK derivatives, brought information about the structure they adopted in living cells.

First, the fusion of GFP to the TK parts did not induce a substantial alteration of the tertiary structure of the GFP protein, because the lifetime of the GFP chromophore did not change significantly. Indeed, the fluorescence lifetime of the GFP chromophore is very sensitive to folding (Chattoraj et al., 1996) or to tertiary modifications (Volkmer et al., 2000). Interestingly, no additional shorter fluorescence lifetime was found upon aggregation of $TK_{366}GFP$, meaning that GFP was not misfolded. It is possible that this result applies to the TK protein domain too, because it was recently shown that the folding of the GFP domain fused downstream of a partner protein is directly related to the folding of the upstream protein domain (Waldo et al., 1999).

Second, the oligomeric state of the GFP-tagged TK derivatives could be detected in subcellular regions of a living cell, even when the amount of protein was very low, as occurred with $TK_{366}GFP$ in the cytoplasm. Fluorescence depolarization due to energy transfer resulting from homo-FRET appears to constitute a very sensitive method for following homo-dimer formation. The fast relaxation time of 2.4 ns (resulting from the transfer rate between the two GFP chromophores) and the r_∞ value (allowing the mutual orientation of interacting GFP chromophores to be determined) are comparable for aggregates and for weak and diffuse cytoplasmic fluorescence in cells containing aggregates. This result rules out the possibility that homo-transfer could have arisen from an effect of high protein concentration. It reveals the oligomerization state, i.e., dimerization

of $TK_{366}GFP$. Moreover, the occurrence of a homo-dimer and not a larger oligomer is suggested by the fact that the fluorescence depolarization was not total, indicating that several steps of energy migration are improbable, even within subcellular aggregates. It is likely that these structures involved cellular protein(s) that stabilize the micron-size aggregates containing fluorescent dimers.

Quantification of homo-FRET was done by fitting fluorescence anisotropy decays to Eq. 16, which provides the rate of energy transfer and the orientation between the interacting dipoles. From these measurements, dimers of $TK_{366}GFP$ could be characterized in terms of mutual orientation and maximum distance (70 Å) between the GFPs. In the $TK_{366}GFP$ construct, the C-terminal α helix (α_{12}) of the TK is shortened by 10 amino acids. This α_{12} helix has been shown to be one of the four helices interacting at the monomer-monomer interface in the crystal of thymidine kinase (Wild et al., 1997). The results obtained indicate that the deletion of part of the α_{12} helix is not sufficient to impede the dimerization of this GFP-tagged TK derivative.

Two questions that are relevant to the physiological aspect remain unanswered. First, why was the protein $TK_{366}GFP$ stabilized in the monomer form at least 1 day before dimerization? And second, why did the dimers aggregate? The fact that these two characteristics of $TK_{366}GFP$ behavior in living cells are independent of the concentration of cellular fusion protein suggests that specific cellular mechanisms may be involved.

Time-resolved fluorescence anisotropy microscopy opens a new avenue for obtaining unique structural parameters on proteins in the living cell, such as monomer-dimer transitions and estimation of inter-molecular distances.

We are indebted to P. Denjean for laser adjustments and skillful help and Drs. M. J. Masse and R. d'Ari for critical reading of the manuscript.

This work was supported by grants from the European Union (BIO4 CT97 2177), the Association pour la Recherche sur le Cancer, Physique et Chimie du Vivant, the Groupement des Entreprises Françaises de Lutte contre le Cancer, and le Laboratoire Glaxo Wellcome. M. Tramier was supported by a European Union fellowship.

REFERENCES

Axelrod, D. 1979. Carbocyanine dye orientation in red cell membrane studied by microscopic fluorescence polarization. *Biophys. J.* 26: 557–574.

Axelrod, D. 1989. Fluorescence polarization microscopy. *Methods Cell Biol.* 30:333–352.

Bastiaens, P. I. H., and A. Squire. 1999. Fluorescence lifetime imaging microscopy: spatial resolution of biochemical processes in the cell. *Trends Cell Biol.* 9:48–52.

Bastiaens, P. I. H., A. van Hoek, J. A. E. Benen, J.-C. Brochon, and A. J. W. G. Visser. 1992. Conformational dynamics and intersubunit energy transfer in wild-type and mutant lipoamide dehydrogenase from *Azotobacter vinelandii*: a multidimensional time-resolved polarized fluorescence study. *Biophys. J.* 63:839–853.

Bergström, F., P. Hägglöf, J. Karolin, T. Ny, and L. B.-Å. Johansson. 1999. The use of site-directed fluorophore labeling and donor-donor energy migration to investigate solution structure and dynamics in proteins. *Proc. Natl. Acad. Sci. U.S.A.* 96:12477–12481.

Blackman, S. M., D. W. Piston, and A. H. Beth. 1998. Oligomeric state of human erythrocyte band 3 measured by fluorescence resonance energy homotransfer. *Biophys. J.* 75:1117–1130.

Cantor, C. R., and P. R. Schimmel. 1980. Biophysical Chemistry II. W. H. Freeman, San Francisco.

Chattoraj, M., B. A. King, G. U. Bublitz, and S. G. Boxer. 1996. Ultra-fast excited state dynamics in green fluorescent protein: multiple states and proton transfer. *Proc. Natl. Acad. Sci. U.S.A.* 93:8362–8367.

Coppey-Moisan, M., J. Delic, H. Magdelénat, and J. Coppey. 1994. Principle of digital imaging microscopy. *Methods Mol. Biol.* 33:359–393.

Creemers, T. M. H., A. J. Lock, V. Subramaniam, T. M. Jovin, and S. Völker. 2000. Photophysics and optical switching in green fluorescent protein mutants. *Proc. Natl. Acad. Sci. U.S.A.* 97:2974–2978.

Emmanouilidou, E., A. G. Teschemacher, A. E. Pouli, L. I. Nicholls, E. P. Seward, and G. A. Rutter. 1999. Imaging Ca^{2+} concentration changes at the secretory vesicle surface with a recombinant targeted cameleon. *Curr. Biol.* 9:915–918.

Fetzer, J., M. Michael, T. Bohner, R. Hofbauer, and G. Folkers. 1994. A fast method for obtaining highly pure recombinant herpes simplex virus type 1 thymidine kinase. *Protein Exp. Purif.* 5:432–441.

Förster, T. 1948. Zwischenmolekulare energiewanderung und fluoreszenz. *Ann. Phys.* 2:55–75.

Hink, M. A., R. A. Griep, J. W. Borst, A. van Hoek, M. H. M. Eppink, A. Schots, and A. J. W. G. Visser. 2000. Structural dynamics of green fluorescent protein alone and fused with a single chain Fv protein. *J. Biol. Chem.* 275:17556–17560.

Llopis, J., S. Westin, M. Ricote, J. Wang, C. Y. Cho, R. Kurokawa, T. M. Mullen, D. W. Rose, M. G. Rosenfeld, R. Y. Tsien, and C. K. Glass. 2000. Ligand-dependent interactions of coactivators steroid receptor coactivator-1 and peroxisome proliferator-activated receptor binding protein with nuclear hormone receptors can be imaged in live cells and are required for transcription. *Proc. Natl. Acad. Sci. U.S.A.* 97: 4363–4368.

Mahajan, N. P., K. Linder, G. Berry, G. W. Gordon, R. Heim, and B. Herman. 1998. Bcl-2 and bax interactions in mitochondria probed with green fluorescent protein and fluorescence resonance energy transfer. *Nat. Biotechnol.* 16:547–552.

Nagai, Y., M. Miyazaki, R. Aoki, T. Zama, S. Inouye, K. Hirose, M. Iino, and M. Hagiwara. 2000. A fluorescent indicator for visualizing cAMP-induced phosphorylation in vivo. *Nat. Biotechnol.* 18:313–316.

Ng, T., A. Squire, G. Hansra, F. Bornancin, C. Prevostel, A. Hanby, W. Harris, D. Barnes, S. Schmidt, H. Mellor, P. I. Bastiaens, and P. J. Parker. 1999. Imaging protein kinase Cα activation in cells. *Science.* 283:2085–2089.

O'Connor, D. V., and D. Phillips. 1984. Time-Correlated Single Photon Counting. Academic Press, New York.

Pepperkok, R., A. Squire, S. Geley, and P. I. H. Bastiaens. 1999. Simultaneous detection of multiple green fluorescent proteins in live cells by fluorescence lifetime imaging microscopy. *Curr. Biol.* 9:269–272.

Runnels, L. W., and S. F. Scarlata. 1995. Theory and application of fluorescence homotransfer to melittin oligomerization. *Biophys. J.* 69: 1569–1583.

Stryer, L. 1978. Fluorescence energy transfer as a spectroscopic ruler. *Annu. Rev. Biochem.* 47:819–846.

Swaminathan, R., C. P. Hoang, and A. S. Verkman. 1997. Photobleaching recovery and anisotropy decay of green fluorescent protein GFP-S65T in solution and cells: cytoplasmic viscosity probed by green fluorescent protein translational and rotational diffusion. *Biophys. J.* 72:1900–1907.

Tanaka, F., and N. Mataga. 1979. Theory of time-dependent photoselection in interacting fixed systems. *Photochem. Photobiol.* 29: 1091–1097.

Tramier, M., K. Kemnitz, C. Durieux, J. Coppey, P. Denjean, R. B. Pansu, and M. Coppey-Moisan. 2000. Restrained torsional dynamics of nuclear DNA in living proliferative mammalian cells. *Biophys. J.* 78: 2614–2627.

Vanderklish, P. W., L. A. Krushel, B. H. Holst, J. A. Gally, K. L. Crossin, and G. M. Edelman. 2000. Marking synaptic activity in dendritic spines with a calpain substrate exhibiting fluorescence resonance energy transfer. *Proc. Natl. Acad. Sci. U.S.A.* 97:2253–2258.

Van der Meer, B. W., I. G. Coker, and S.-Y. S. Chen. 1994. Resonance Energy Transfer: Theory and Data. VCH, New York.

Varma, R., and S. Mayor. 1998. GPI-anchored proteins are organized in submicron domains at the cell surface. *Nature.* 394:798–801.

Volkmer, A., V. Subramaniam, D. J. S. Birch, and T. M. Jovin. 2000. One- and two-photon excited fluorescence lifetimes and anisotropy decays of green fluorescent proteins. *Biophys. J.* 78:1589–1598.

Waldman, A. S., E. Haeusslein, and G. Milman. 1983. Purification and characterization of herpes simplex virus (type 1) thymidine kinase produced in *Escherichia coli* by a high efficiency expression plasmid utilizing a lambda PL promoter and cI857 temperature-sensitive repressor. *J. Biol. Chem.* 258:11571–11575.

Waldo, G. S., B. M. Standish, J. Berendzen, and T. C. Terwilliger. 1999. Rapid protein-folding assay using green fluorescent protein. *Nat. Biotechnol.* 17:691–695.

Ward, W. W., H. J. Prentice, A. F. Roth, C. W. Cody, and S. C. Reeves. 1982. Spectral perturbations of the *Aequorea* green-fluorescent protein. *Photochem. Photobiol.* 35:803–808.

Weber, G. 1954. Dependence of polarization of the fluorescence on the concentration. *Trans. Faraday Soc.* 50:552–555.

Wild, K., T. Bohner, G. Folkers, and G. E. Schulz. 1997. The structures of thymidine kinase from *Herpes simplex* virus type 1 in complex with substrates and a substrate analogue. *Protein Sci.* 6:2097–2106.

Wilczynska, M., M. Fa, J. Karolin, P. I. Ohlsson, L. B.-A. Johansson, and T. Ny. 1997. Structural insights into serpin protease complexes reveal the inhibitory mechanism of serpins. *Nat. Struct. Biol.* 4:354–357.